

**PARTIAL RELAXATION OF C^0 VERTEX CONTINUITY OF STRESSES OF
CONFORMING MIXED FINITE ELEMENTS FOR THE ELASTICITY
PROBLEM**

JUN HU AND RUI MA

ABSTRACT. With two benchmark examples, this paper presents a general method to deal with stress internal/boundary conditions for conforming mixed elements for elasticity problems where vertex degrees of freedom are usually involved. The main idea is to partially relax the C^0 continuity of discrete stresses at these vertices under consideration. More precisely, only the normal components of the discrete stresses are required to be continuous across the low dimensional subfaces where these vertices are located. This paper also extends the method to construct nested mixed finite elements on adaptive meshes and proves convergence and optimality of the adaptive algorithm.

Keywords. linear elasticity, nested mixed finite element, adaptive algorithm

AMS subject classifications. 65N30, 74B05.

1. INTRODUCTION

The problems that are most frequently solved in scientific and engineering computing may probably be the elasticity equations. The finite element method (FEM) was invented in analyzing the stress of the elastic structures in the 1950s. The mixed FEM within the Hellinger-Reissner (H-R) principle for elasticity yields a direct stress approximation since it takes both the stress and displacement as an independent variable; while the displacement FEM only gives an indirect stress approximation. Hu, a founder of the celebrated Hu-Washizu principle for elasticity, pointed out that, the H-R principle is more general than both the minimum potential and complementary energy principles, and is much fitter for numerical solutions [13]. Indeed, the mixed FEM can be free of locking for nearly incompressible materials, and be applied to plastic materials, and approximate both the equilibrium and traction boundary conditions more accurate. However, the symmetry of the stress plus the stability conditions make the design of the mixed FEM for elasticity surprisingly hard, which has been regarded as a long standing open problem [2]. In fact, Four decades of searching for mixed finite elements for elasticity beginning in the 1960s did not yield any stable elements with polynomial shape functions [D. N. Arnold, Proceedings of the ICM, Vol. I : Plenary Lectures and Ceremonies (2002)].

Since the 1960s, many mathematicians have worked on this problem but compromised to weakly symmetric elements [3, 4, 6], or composite elements [21]. In 2002, using the elasticity complexes, Arnold and Winther designed the first family of symmetric mixed elements with polynomial shape functions on triangular grids in 2D [5] which was extended to tetrahedral grids in 3D [2] and to rectangular grids in 2D [1]. Recently, the first author

The first author was supported by NSFC projects 11271035, 91430213 and 11421101.

and his collaborators developed a new framework to design and analyze the mixed FEM of elasticity problems, which yields optimal symmetric mixed FEMs. In addition, those elements are very easy to implement since their basis functions, based on those of the scalar Lagrange elements, can be explicitly written down by hand. The main ingredients of this framework are a structure of the discrete stress space on both simplicial and product grids, two basic algebraic results, and a two-step stability analysis method, see more details in [14, 15, 17, 18, 19].

The $H(\text{div})$ conformity of discrete stresses only requires the continuity of normal components of symmetric matrix-valued piecewise polynomials. However, due to the constraint of the symmetry, all the conforming mixed elements mentioned above impose the C^0 continuity of discrete stresses at vertices. This introduces some inconsistency errors when discretizing some interface problems and stress boundary condition problems. Besides, because of the C^0 continuity of discrete stresses at vertices, the stress space on the coarse mesh is not a subspace of that on the fine mesh, which causes the difficulty of the convergence analysis of adaptive algorithms for the aforementioned elements, though there are some a posteriori error estimators of two families of triangular mixed elements of [5, 14, 17] in literature, see [9, 12].

With two benchmark examples, this paper proposes a method to cure the problems caused by the vertex degrees of freedom. This paper mainly focuses on the two dimensional elements from [5, 14, 17], and give a comment for the three dimensional case in Section 3. The first example is an interface problem with a piecewise constant stress whose normal components is continuous across a line. However the pure tangential component is discontinuous across the same line. Because of the C^0 continuity of discrete stresses at the vertices on this line, even for such a simple case, the two mixed finite element methods of [5, 14, 17] cannot compute the exact stress. The remedy is to relax the C^0 continuity of discrete stresses at all vertices on this line. More precisely, the degree of freedom of the pure tangential component is split into two separate degrees of freedom. As a result, the stress space is enriched with some functions with discontinuous tangential components across this line and the exact stress is included in the extended stress space. The second example is Cook's membrane problem whose mixed element methods should impose the stress boundary condition. In order to impose general stress boundary conditions on two edges which intersect at a corner under consideration, it requires four degrees of freedom at the corner vertex. However, both elements of [5, 14, 17] can only provide three. To handle such a case, the authors of [8] compromised a least square method to obtain some approximations of the stress boundary condition. In this paper, the method for the first example is extended to deal with this case. By splitting the triangle at the corner into two sub-triangles and relaxing the continuity of the pure tangential component across these two triangles, it eventually leads to four degrees of freedom at the corner vertex. The numerical results on two benchmark examples show that this remedy reduces largely both the L^2 errors of the stress and displacement on coarse meshes. Moreover, the numerical experiment of the adaptive version of the mixed element of [14, 17] for Cook's membrane problem demonstrates that, after the remedy, it performs much better at the first several refinement loops.

The second purpose of the paper is to design nested mixed conforming finite elements on adaptive meshes. The crucial idea is motivated by the method developed in the first example and the fact that in the mesh refinement of adaptive algorithms, the new vertices produced by the new vertex bisection are always located at the middle points of some edges of the previous level mesh. Hence the C^0 continuity of discrete stresses in [5, 14, 17] can

be relaxed at all the new vertices by splitting the degrees of freedom of the pure tangential components with respect to the edges of the previous level mesh into two separate degrees of freedom. The resulting extended stress spaces then have four degrees of freedom instead of three at all new vertices and are nested on adaptive meshes. The nestedness property enables to generalize the framework for the vector and non-symmetric mixed elements in [16] to prove the optimal convergence rates of adaptive algorithms for the symmetric mixed elements. The analysis is established for the mixed element from [14, 17] with the a posteriori error estimator of [12] in the adaptive algorithm. We remark that it can be extended to the Arnold-Winther element [5].

The rest of the paper is organized as follows. Section 2 introduce notation in this paper and the mixed element on triangular meshes [14, 17], including its degrees of freedom and basis functions. Section 3 presents two examples, in which it requires to deal with the vertex degrees of freedom. This section proposes a method to partially relax the C^0 continuity at these vertices. Section 4 designs nested mixed finite elements on adaptive meshes and prove optimality of the corresponding adaptive algorithm. Numerical experiments are presented in Section 5.

2. PRELIMINARIES

Let $\Omega \subset \mathbb{R}^2$ be a bounded polygonal domain with boundary $\Gamma := \partial\Omega = \Gamma_D \cup \Gamma_N$, $\Gamma_D \cap \Gamma_N = \emptyset$. Let $H^k(\omega; X)$ denote the Soblev space consisting of functions with domain ω , taking values in the finite-dimensional vector space X , and with all derivatives of order at most k square-integrable. Let $L^2(\omega; X)$ denote the space of functions which are square-integrable. For our purposes, the range space X will be either $\mathbb{S} :=$ symmetric $\mathbb{R}^{2 \times 2}$, \mathbb{R}^2 , or \mathbb{R} . Let $H(\text{div}, \omega; \mathbb{S})$ consist of square-integrable symmetric matrix fields with square-integrable divergence. Let $\|\cdot\|_{k,\omega}$ represent the norm of $H^k(\omega)$, and $(\cdot, \cdot)_\omega$ represent as usual, the L^2 inner product on the domain ω , the subscript ω is omitted when $\omega = \Omega$. $\langle \cdot, \cdot \rangle_\Gamma$ represents the L^2 inner product on the boundary Γ .

Given $f \in L^2(\Omega; \mathbb{R}^2)$, $u_D \in H^1(\Omega; \mathbb{R}^2)$ and $g \in L^2(\Gamma_N; \mathbb{R}^2)$, the linear elasticity problem with mixed boundary conditions within a stress-displacement form reads: Seek $(\sigma, u) \in \Sigma_g \times V$ such that

$$(2.1) \quad \begin{cases} (A\sigma, \tau) + (\text{div}\tau, u) = \langle u_D, \tau n \rangle_{\Gamma_D} & \text{for all } \tau \in \Sigma_0, \\ (\text{div}\sigma, v) = (f, v) & \text{for all } v \in V \end{cases}$$

with

$$\Sigma_0 := \{\sigma \in H(\text{div}, \Omega; \mathbb{S}) \mid \int_{\Gamma_N} \psi \cdot (\sigma n) ds = 0, \text{ for all } \psi \in \mathcal{D}(\Gamma_N; \mathbb{R}^2)\},$$

$$\Sigma_g := \{\sigma \in H(\text{div}, \Omega; \mathbb{S}) \mid \int_{\Gamma_N} \psi \cdot (\sigma n) ds = \int_{\Gamma_N} \psi \cdot g ds, \text{ for all } \psi \in \mathcal{D}(\Gamma_N; \mathbb{R}^2)\}.$$

Here \mathcal{D} denotes the space of test functions and n denotes the outnormal of $\partial\Omega$. Define the norm $\|\cdot\|_A := (A\cdot, \cdot)^{1/2}$.

Suppose that Ω is subdivided by a family of shape regular triangular meshes \mathcal{T}_h (with the mesh size h). Given any integer k , let $P_k(\omega; X)$ denote the space of polynomials over ω of total degrees not greater than k , taking values in the finite-dimensional vector space X . Let \mathbf{x}_i ($1 \leq i \leq 3$) denote the vertices of triangle $K \in \mathcal{T}_h$, λ_i denote the barycentric coordinates with respect to \mathbf{x}_i , and $t_{i,j} = \mathbf{x}_j - \mathbf{x}_i$ denote the tangent vector of edge $\mathbf{x}_i\mathbf{x}_j$.

The remaining of this section recalls the conforming mixed element from [14, 17]. With symmetric matrices $\mathbb{T}_{i,j} := t_{i,j}t_{i,j}^T$, $1 \leq i < j \leq 3$ of rank one, define an $H(\text{div}, K; \mathbb{S})$ bubble

function space

$$\Sigma_{K,k,b} := \sum_{1 \leq i < j \leq 3} \lambda_i \lambda_j P_{k-2}(K; \mathbb{R}) \mathbb{T}_{i,j}.$$

Then the discrete stress space Σ_h of $k \geq 3$ has the following crucial structure:

$$(2.2) \quad \begin{aligned} \Sigma_h := & \{ \sigma \in H(\operatorname{div}, \Omega; \mathbb{S}) \mid \sigma = \sigma_c + \sigma_b, \sigma_c \in H^1(\Omega; \mathbb{S}), \\ & \sigma_c|_K \in P_k(K; \mathbb{S}), \sigma_b|_K \in \Sigma_{K,k,b}, \forall K \in \mathcal{T}_h \}. \end{aligned}$$

A matrix field $\tau \in P_k(K; \mathbb{S})$ can be uniquely determined by the degrees of freedom from (1), (2) and (3) (see Figure 2.1 with solid points and arrows for $k = 3$):

- (1) the values of τ at three vertices,
- (2) for edge e with unit tangential vector t_e and unit normal vector n_e , the mean moments of degree at most $k - 2$ over e of $n_e \tau n_e^T$, $t_e^T \tau n_e$,
- (3) the values $\int_K \tau : \theta \, dx$ for any $\theta \in \Sigma_{K,k,b}$.

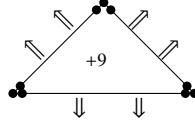


FIGURE 2.1. Degrees of freedom for Σ_h of $k = 3$

Given edge e , define $\mathbb{T}_e := t_e t_e^T$ and $\mathbb{T}_{e,j}^\perp$ with $j = 1, 2$ such that

$$(2.3) \quad \mathbb{T}_{e,1}^\perp = n_e n_e^T, \mathbb{T}_{e,2}^\perp = n_e t_e^T + t_e n_e^T, \text{ therefore, } \mathbb{T}_{e,j}^\perp : \mathbb{T}_e = 0 \text{ and } \mathbb{T}_{e,1}^\perp : \mathbb{T}_{e,2}^\perp = 0,$$

and

$$(2.4) \quad \mathbb{T}_1 = \begin{pmatrix} 1 & 0 \\ 0 & 0 \end{pmatrix}, \mathbb{T}_2 = \begin{pmatrix} 0 & 1 \\ 1 & 0 \end{pmatrix}, \text{ and } \mathbb{T}_3 = \begin{pmatrix} 0 & 0 \\ 0 & 1 \end{pmatrix}.$$

Let $\mathcal{X}_{\mathbb{B}}$ denote all interior Lagrangian nodes of all the edges, $\mathcal{X}_{\mathbb{K}}$ denote all interior Lagrangian nodes of all the elements, and $\mathcal{X}_{\mathbb{V}}$ denote all the vertices of \mathcal{T}_h . Given node $\mathbf{x} \in \mathcal{X}_{\mathbb{V}} \cup \mathcal{X}_{\mathbb{B}} \cup \mathcal{X}_{\mathbb{K}}$, let $\phi_{\mathbf{x}}$ be its associated nodal basis function. The basis functions of Σ_h can be classified into four classes:

- (1) Vertex-based basis functions. Given vertex $\mathbf{x} \in \mathcal{X}_{\mathbb{V}}$, its three associated basis functions of Σ_h read

$$\tau_{V,\mathbf{x},i} = \phi_{\mathbf{x}} \mathbb{T}_i, i = 1, 2, 3.$$

- (2) Volume-based basis functions. Given node $\mathbf{x} \in \mathcal{X}_{\mathbb{K}}$ inside K , its three associated basis functions of Σ_h read

$$\tau_{K,\mathbf{x},i} = \phi_{\mathbf{x}} \mathbb{T}_i, i = 1, 2, 3.$$

- (3) Edge-based basis functions with nonzero fluxes. Given node $\mathbf{x} \in \mathcal{X}_{\mathbb{B}}$ on edge e , its two associated basis functions with nonzero fluxes of Σ_h read

$$\tau_{e,\mathbf{x},i}^{(nb)} = \phi_{\mathbf{x}} \mathbb{T}_{e,i}^\perp, i = 1, 2.$$

- (4) Edge-based bubble functions. Given node $\mathbf{x} \in \mathcal{X}_{\mathbb{B}}$ on edge e which is shared by elements K_1 and K_2 , its bubble functions in Σ_h read

$$\tau_{e,\mathbf{x},i}^{(b)} = \phi_{\mathbf{x}|_{K_i}} \mathbb{T}_e, i = 1, 2.$$

The displacement space is the full C^{-1} - P_{k-1} space

$$(2.5) \quad V_h := \{v \in L^2(\Omega; \mathbb{R}^2) \mid v|_K \in P_{k-1}(K; \mathbb{R}^2) \text{ for all } K \in \mathcal{T}_h\}.$$

Let $\Sigma_{g,h} := \Sigma_g \cap \Sigma_h$ and $\Sigma_{0,h} := \Sigma_0 \cap \Sigma_h$. The mixed finite element method seeks $(\sigma_h, u_h) \in \Sigma_{g,h} \times V_h$ such that

$$(2.6) \quad \begin{cases} (A\sigma_h, \tau_h) + (\operatorname{div}\tau_h, u_h) = \langle u_D, \tau_h n \rangle_{\Gamma_D} & \text{for all } \tau_h \in \Sigma_{0,h}, \\ (\operatorname{div}\sigma_h, v_h) = (f, v_h) & \text{for all } v_h \in V_h. \end{cases}$$

3. METHODOLOGY

This section introduces a method to partially relax C^0 continuity of the discrete stresses at these vertices under consideration.

3.1. Interface problem with a discontinuous pure tangential stress. Let $x = (x_1, x_2)^T$.

Consider a piecewise constant stress $\sigma = \begin{pmatrix} \sigma_{11} & 0 \\ 0 & 0 \end{pmatrix}$ with a discontinuous pure tangential component σ_{11} across $x_2 = 0.5$ depicted in Figure 3.1(a). Suppose that the intersection of any edge of \mathcal{T}_h with $x_2 = 0.5$ is an empty set, a vertex or the edge itself. Recall the stress space Σ_h in (2.2). Since any matrix-valued function in Σ_h is C^0 continuous at each vertex of \mathcal{T}_h . Even for such a simple case, the mixed finite element method (2.6) cannot achieve the exact stress due to $\sigma \notin \Sigma_h$.

Given a vertex \mathbf{a} on $x_2 = 0.5$, the three circles in Figure 3.1(a) represent the three vertex degrees of freedom of Σ_h at \mathbf{a} . The corresponding basis functions read

$$(3.1) \quad \phi_{\mathbf{a}} \begin{pmatrix} 1 & 0 \\ 0 & 0 \end{pmatrix}, \phi_{\mathbf{a}} \begin{pmatrix} 0 & 1 \\ 1 & 0 \end{pmatrix}, \phi_{\mathbf{a}} \begin{pmatrix} 0 & 0 \\ 0 & 1 \end{pmatrix}.$$

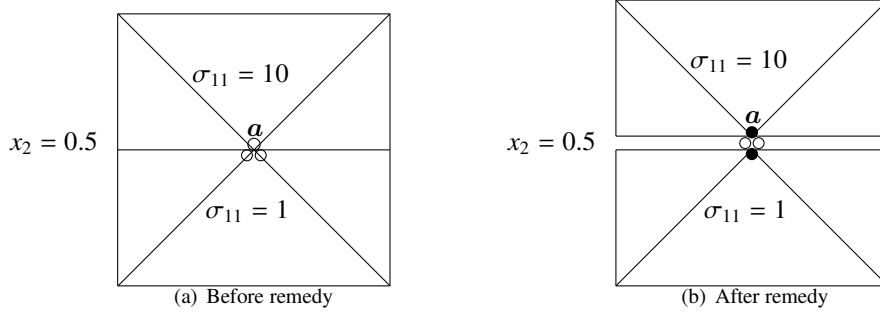
Note that the $H(\operatorname{div})$ conformity only imposes normal continuity across edges in contrast to the pure tangential continuity across edges. It is possible to partially relax C^0 vertex continuity. The remedy is to split the degree of freedom at \mathbf{a} with respect to the pure tangential component along $x_2 = 0.5$ into two degrees of freedom shared by the upper plane and lower plane, respectively. The corresponding basis functions are defined by replacing the first basis function in (3.1) with the following two new functions

$$\phi_{\mathbf{a}|_{x_2 \geq 0.5}} \begin{pmatrix} 1 & 0 \\ 0 & 0 \end{pmatrix}, \phi_{\mathbf{a}|_{x_2 \leq 0.5}} \begin{pmatrix} 1 & 0 \\ 0 & 0 \end{pmatrix}.$$

Here the function $\phi_{\mathbf{a}|_{x_2 \geq 0.5}}$ is globally defined in Ω by extended zero to $x_2 < 0.5$, and $\phi_{\mathbf{a}|_{x_2 \leq 0.5}}$ is similarly defined. The two solid points in Figure 3.1 represent the two new separate degrees of freedom; the two circles represent the degrees of freedom with respect to normal components and their basis functions are the last two functions in (3.1). Deal with all vertices on $x_2 = 0.5$ analogously. An extended stress space $\widetilde{\Sigma}_h$ is then constructed by enriching Σ_h with all the new functions whose pure tangential component are discontinuous at one vertex on $x_2 = 0.5$. It can be easily checked that $\widetilde{\Sigma}_h$ is still $H(\operatorname{div})$ conforming and $\Sigma_h \subset \widetilde{\Sigma}_h$.

Consider the interpolation of σ in $\widetilde{\Sigma}_h$. Let the interpolation $I_h \sigma_{11}$ equal to 1 at vertex \mathbf{a} in each element below $x_2 = 0.5$, and 10 in each element above. Thus $I_h \sigma_{11} = \sigma_{11}$. Since the computing error is less than the interpolation error, the mixed finite element method with the extended stress space $\widetilde{\Sigma}_h$ computes the exact stress.

Remark 3.1. Since $\Sigma_h \subset \widetilde{\Sigma}_h$ and $\operatorname{div}\widetilde{\Sigma}_h \subset V_h$, a similar analysis of [14, 17] shows that the extended stress space $\widetilde{\Sigma}_h$ and the displacement space V_h in (2.5) are stable mixed finite

FIGURE 3.1. Degrees of freedom at vertex a

elements. It also holds for the mixed elements constructed later in Subsect. 3.2 and Section 4. In addition, the idea in this example can be applied to the Arnold-Winther element. Suppose the basis functions τ_k , $1 \leq k \leq 3$ are computed to vanish at the other degrees of freedom and satisfy

$$\tau_1(\mathbf{a}) = \begin{pmatrix} 1 & 0 \\ 0 & 0 \end{pmatrix}, \quad \tau_2(\mathbf{a}) = \begin{pmatrix} 0 & 1 \\ 1 & 0 \end{pmatrix}, \quad \tau_3(\mathbf{a}) = \begin{pmatrix} 0 & 0 \\ 0 & 1 \end{pmatrix}.$$

Split τ_1 into two separate functions

$$\tau_1^+ = \tau_1|_{x_2 \geq 0.5}, \quad \tau_1^- = \tau_1|_{x_2 \leq 0.5},$$

Then, $\tau_1^+, \tau_1^-, \tau_2$ and τ_3 are the new basis functions associated with the degrees of freedom at \mathbf{a} .

3.2. Cook's membrane problem with general stress boundary conditions. The underlying domain is a quadrilateral with vertices at $(0, 0)$, $(48, 44)$, $(48, 60)$ and $(0, 44)$ shown in 3.2. Suppose n denotes the outnormal of the domain. It is fixed ($u = 0$) at the left edge ($x_1 = 0$) while a uniform traction force pointing upwards ($\sigma n = (0, 1)^T$) is applied at the right edge ($x_1 = 48$). At the remaining part of the boundary it is kept in equilibrium ($\sigma n = 0$). At the corner vertices \mathbf{a} and \mathbf{b} , there exist inconsistent boundary conditions.

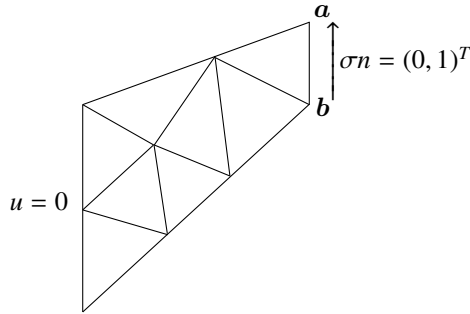


FIGURE 3.2. Cook's membrane problem

To impose the Neumann boundary conditions that $\sigma_h \in \Sigma_g$, for each vertex \mathbf{x} on the Neumann boundary $\sigma_h(\mathbf{x})n = g(\mathbf{x})$ for the three unknowns of $\sigma_h(\mathbf{x})$. However, this cannot

be satisfied if there exist general Neumann conditions at \mathbf{a} and \mathbf{b} . In fact, such a case needs $\sigma_h(\mathbf{x})n_1 = g_1(\mathbf{x})$ and $\sigma_h(\mathbf{x})n_2 = g_2(\mathbf{x})$, where n_1 and n_2 denote the outer unit normal vectors of the two incident edges. In general, this over-determined system does not have a solution. The least square constraint was employed in [8] to deal with this case. This paper extends the method in Subset. 3.1 to allow for an exact Neumann boundary conditions at the corner.

Given a corner vertex \mathbf{a} shown in Figure 3.3(a), it is impossible to relax the C^0 continuity at \mathbf{a} in one element K since the degrees of freedom are over-determined. Divide K into a patch consisting of two triangles K_+ and K_- such that $K = K_+ \cup K_-$ and $e = K_+ \cap K_-$ as in Figure 3.3(b). As explained in Subset. 3.1, the pure tangential component does not have to be continuous across e at \mathbf{a} . Therefore, one can divide this degree of freedom into two separate degrees of freedom in K_+ and K_- , respectively. In Figure 3.3(c), the solid points represent these two separate degrees of freedom and the two circles represent the degrees of freedom of normal components across e . In order to impose the Neumann boundary conditions or the normal continuity on e_+ and e_- , it requires to modify the four degrees of freedom in Figure 3.3(c) to two normal degrees of freedom on e_+ and two normal degrees of freedom on e_- , see the arrows in Figure 3.3(d). This is workable as long as e_+ is not parallel to e_- . In fact, if e_+ is parallel to e_- , one of the normal component across e is the pure tangential component along e_1 , which has no contribution to the normal components across e_+ .

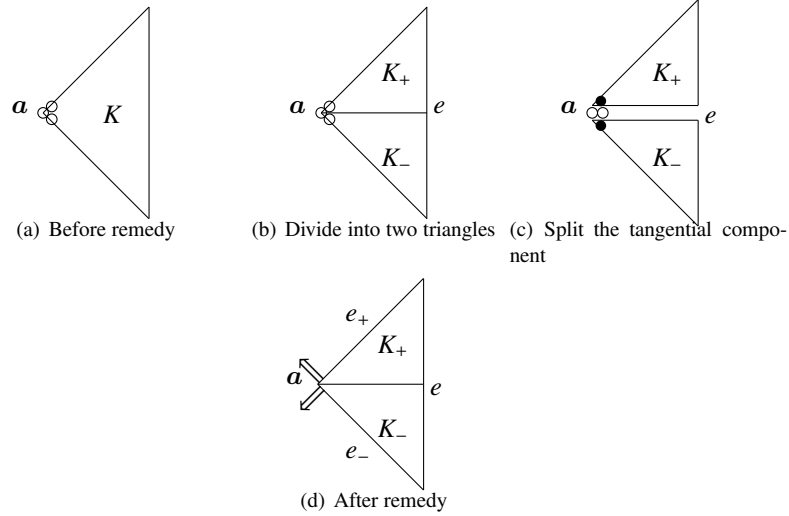


FIGURE 3.3. Degrees of freedom at corner vertex \mathbf{a}

Moreover, the four new basis functions associated with the four degrees of freedom shown in Figure 3.3(d) can be displayed as follows:

$$(3.2) \quad \begin{aligned} \tau_1 &= \phi_{\mathbf{a}} \begin{cases} \mathbb{T}_{e_{+,1}}^{\perp} + c_1 \mathbb{T}_{e_+} & \text{on } K_+ \\ d_1 \mathbb{T}_{e_-} & \text{on } K_- \end{cases}, \quad \tau_2 = \phi_{\mathbf{a}} \begin{cases} \mathbb{T}_{e_{+,2}}^{\perp} + c_2 \mathbb{T}_{e_+} & \text{on } K_+ \\ d_2 \mathbb{T}_{e_-} & \text{on } K_- \end{cases} \\ \tau_3 &= \phi_{\mathbf{a}} \begin{cases} c_3 \mathbb{T}_{e_+} & \text{on } K_+ \\ \mathbb{T}_{e_{-,1}}^{\perp} + d_3 \mathbb{T}_{e_-} & \text{on } K_- \end{cases}, \quad \tau_4 = \phi_{\mathbf{a}} \begin{cases} c_4 \mathbb{T}_{e_+} & \text{on } K_+ \\ \mathbb{T}_{e_{-,2}}^{\perp} + d_4 \mathbb{T}_{e_-} & \text{on } K_- \end{cases} \end{aligned}$$

with the Lagrange basis function $\phi_{\mathbf{a}}$ associated to the node \mathbf{a} and the other notation defined in Section 2. Using the normal continuity of the stress across edge e yields the constants c_i, d_i for $1 \leq i \leq 4$. For instance, given the unit normal vector n_e of e , the normal continuity of τ_1 results in the following equations

$$(3.3) \quad (\mathbb{T}_{e_+,1}^\perp + c_1 \mathbb{T}_{e_+}) n_e = d_1 \mathbb{T}_{e_-} n_e.$$

Recall the definition of the matrix $\mathbb{T}_e = t_e t_e^T$ for edge e with unit tangential vector t_e and the analogies for $\mathbb{T}_{e_+}, \mathbb{T}_{e_-}$. Assuming $t_{e_+} = (a, b)^T$, define its perpendicular row vector by $t_{e_+}^\perp = (b, -a)$; $t_{e_-}^\perp$ is similar defined for t_{e_-} . Let $t_{e_+} \wedge t_{e_-}$ denote the determinant of the matrix (t_{e_+}, t_{e_-}) . Then, elementary computations eventually lead to

$$(\mathbb{T}_{e_+} n_e, -\mathbb{T}_{e_-} n_e)^{-1} = ((t_{e_+}^T n_e) t_{e_+}, -(t_{e_-}^T n_e) t_{e_-})^{-1} = \frac{1}{t_{e_+} \wedge t_{e_-}} \begin{pmatrix} \frac{1}{t_{e_+}^T n_e} t_{e_+}^\perp \\ \frac{1}{t_{e_-}^T n_e} t_{e_-}^\perp \end{pmatrix}$$

Therefore, it is straightforward that there always exist unique solutions c_1, d_1 to (3.3) unless e_+ is parallel to e_- .

Remark 3.2. Note that in this example it requires an even number of triangles around a corner vertex to relax the C^0 continuity at this node. This constraint on the mesh can be circumvented by dividing each triangle around the corner into three sub-triangles shown in Figure 3.4. The third numerical example in Section 5 explains a special mesh refinement in adaptive algorithms to avoid generating triangles with small angles.

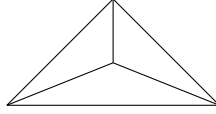


FIGURE 3.4. Element refinement

Remark 3.3. As for the Arnold-Winther element, compute three symmetric matrix-valued basis functions $\xi_k^+, 1 \leq k \leq 3$ which vanish at the other degrees of freedom on element K_+ and satisfy

$$\xi_1^+(\mathbf{a}) = \mathbb{T}_{e_+,1}^\perp, \quad \xi_2^+(\mathbf{a}) = \mathbb{T}_{e_+,2}^\perp, \quad \xi_3^+(\mathbf{a}) = \mathbb{T}_{e_+},$$

and the analogies $\xi_k^-, 1 \leq k \leq 3$ associated with K_- . Then, the expressions in (3.2) can be applied similarly.

3.3. Comments for three dimensions. This subsection generalizes to the mixed element on tetrahedral grids [14, 18] and only provides an outline. Apart from the C^0 continuity at vertices, the discrete stresses have some continuity across edges. Like the first example in Subsect. 3.1, if the pure tangential components of the discrete stress are discontinuous across a plane, the degree of freedom of any pure tangential component along the plane at any vertex and any edge on the plane is then split into two separate degrees of freedom. For instance, suppose τ denotes one of these associated basis functions and $x_3 = 0$ denotes the plane, the two new separate basis functions then read

$$\tau_1 = \begin{cases} \tau & x_3 \geq 0 \\ 0 & x_3 < 0 \end{cases} \quad \text{and} \quad \tau_2 = \begin{cases} 0 & x_3 > 0 \\ \tau & x_3 \leq 0. \end{cases}$$

If general stress boundary conditions are imposed on the intersection of three planes, it requires to deal with the degrees of freedom associated with vertices and edges. Given a tetrahedron $K := \mathbf{x}_0\mathbf{x}_1\mathbf{x}_2\mathbf{x}_3$ in Figure 3.5, suppose \mathbf{x}_0 denotes the corner vertex. In order to relax some continuity at vertices and edges, divide K into four sub-tetrahedra with the barycentre \mathbf{x}'_0 . As shown in Subsect. 3.2, the task is to compute the new basis functions associated with vertex \mathbf{x}_0 and edges $\mathbf{x}_0\mathbf{x}_1$, $\mathbf{x}_0\mathbf{x}_2$, $\mathbf{x}_0\mathbf{x}_3$ as those in (3.2) associated with the corner vertex \mathbf{a} . Let n_1 , n_2 and n_3 denote the outnormal of face $F_1 := \mathbf{x}_0\mathbf{x}_2\mathbf{x}_1$, face $F_2 := \mathbf{x}_0\mathbf{x}_1\mathbf{x}_3$ and face $F_3 := \mathbf{x}_0\mathbf{x}_3\mathbf{x}_2$ respectively. Given $1 \leq k \leq 3$, note that there exist

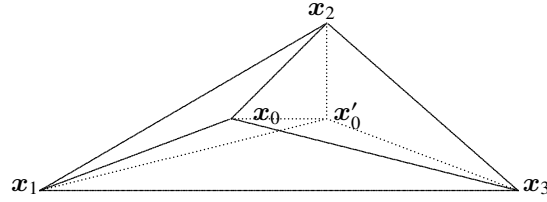


FIGURE 3.5. Tetrahedron K

three independent symmetric matrices $\mathbb{T}_{i,k}$ in each sub-tetrahedron $K_k = \text{conv}(\mathbf{x}'_0 \cup F_k)$ such that $\mathbb{T}_{i,k}n_k = 0$, $1 \leq i \leq 3$ and three symmetric independent matrices $\mathbb{T}_{j,k}^\perp$ such that $\mathbb{T}_{j,k}^\perp : \mathbb{T}_{i,k} = 0$, $1 \leq j \leq 3$. Assume the following expression

$$\tau_{i,1} = \phi_{\mathbf{x}_0} \begin{cases} \mathbb{T}_{i,1}^\perp + \sum_{k=1}^3 c_{k,1} \mathbb{T}_{k,1} & \text{on } K_1, \\ \sum_{k=1}^3 d_{k,1} \mathbb{T}_{k,2} & \text{on } K_2, \\ \sum_{k=1}^3 e_{k,1} \mathbb{T}_{k,3} & \text{on } K_3 \end{cases}$$

with the the Lagrange basis function $\phi_{\mathbf{x}_0}$ associated with \mathbf{x}_0 and nine constants $c_{k,1}, d_{k,1}, e_{k,1}$. It can be easily checked that $\tau_{i,1}n_k|_{F_k} = 0$ for $k = 2, 3$. Using the normal continuity across the interior faces leads to the unique solutions $c_{k,1}, d_{k,1}, e_{k,1}$ as long as any two of F_k , $1 \leq k \leq 3$ do not lie in one plane. Hence $\tau_{i,1}$, $1 \leq i \leq 3$ are three new basis function associated with \mathbf{x}_0 . Similar arguments compute the other six functions associated with the vertex \mathbf{x}_0 .

As for any interior node \mathbf{a} in the edge $\mathbf{x}_0\mathbf{x}_1$, define

$$\xi_{i,1} = \phi_{\mathbf{a}} \begin{cases} \mathbb{T}_{i,1}^\perp + \sum_{k=1}^3 c_{k,1} \mathbb{T}_{k,1} & \text{on } K_1, \\ \sum_{k=1}^3 d_{k,1} \mathbb{T}_{k,2} & \text{on } K_2 \end{cases}$$

with the the Lagrange basis function $\phi_{\mathbf{a}}$ associated with \mathbf{a} and four constants $c_{k,1}, d_{k,1}$. Here it should be careful because the normal continuity across the interior face $\mathbf{x}_1\mathbf{x}'_0\mathbf{x}_0$ only imposes three conditions. Therefore, there exist some $H(\text{div})$ bubble functions on $K_1 \cup K_2$. Let t , t_1 and t_2 denote the tangential vector of edge $\mathbf{x}_0\mathbf{x}_1$, $\mathbf{x}_0\mathbf{x}_2$, $\mathbf{x}_0\mathbf{x}_3$, and let n denote the normal vector of face $\mathbf{x}_1\mathbf{x}'_0\mathbf{x}_0$. The three $H(\text{div})$ bubble functions read

$$\xi_{b,1} = \begin{cases} \phi_{\mathbf{a}} t t^T & \text{on } K_1 \\ 0 & \text{on } K_2 \end{cases}, \quad \xi_{b,2} = \begin{cases} 0 & \text{on } K_1 \\ \phi_{\mathbf{a}} t t^T & \text{on } K_2 \end{cases}, \quad \xi_{b,3} = \begin{cases} \frac{\phi_{\mathbf{a}}}{t_1^T n} (t_1 t^T + t t_1^T) & \text{on } K_1 \\ \frac{\phi_{\mathbf{a}}}{t_2^T n} (t_2 t^T + t t_2^T) & \text{on } K_2 \end{cases}.$$

Actually, $\xi_{b,1}$ (resp. $\xi_{b,2}$) is already the original $H(\text{div})$ bubble function on K_1 (resp. K_2) from [14, 18]. Unless F_1 and F_2 are parallel, there always exist the unique six constants $c_{k,1}, d_{k,1}$ with the constraint of the bubble functions. Hence $\xi_{i,1}$, $1 \leq i \leq 3$ are three new basis function associated with edge $\mathbf{x}_0\mathbf{x}_1$.

4. ADAPTIVITY

4.1. Nested mixed conforming elements on adaptive meshes. The C^0 continuity at vertices leads to the non-nestedness in the sense that the finer stress spaces Σ_h from [5, 14, 17] do not include the coarser stress spaces Σ_H . Hence it is not easy to prove convergence of the corresponding adaptive algorithms. The subsequent parts are devoted to relax C^0 continuity of discrete stress functions at vertices and design nested mixed finite elements on adaptive meshes. The main ingredients are the method employed in the first example in Section 2 and the fact that in the mesh refinement of adaptive algorithms, new vertices generated by the newest vertex bisection are always located at the middle points of some edges of the previous level mesh. For simplicity, this paper only analyzes the mixed conforming element from [14, 17].

Note that each new vertex \mathbf{x} must be a midpoint of some old edge e in \mathcal{T}_H and attach its unit tangential vector to \mathbf{x} and denote as $t_{\mathbf{x}}$. The degree of freedom with respect of the pure tangential component along $t_{\mathbf{x}}$ at \mathbf{x} is separated into two as done in Subsection 3.1. Hence this results in an extended discrete stress space. Suppose \mathcal{T}_0 is the initial mesh and \mathcal{T}_h is a refined mesh. Let $n_{\mathbf{x}}$ denote the unit vector perpendicular to $t_{\mathbf{x}}$. The four basis functions for any vertex $\mathbf{x} \in \mathcal{X}_{\mathbb{V}}(\mathcal{T}_h) \setminus \mathcal{X}_{\mathbb{V}}(\mathcal{T}_0)$ are $\phi_{\mathbf{x}} n_{\mathbf{x}} n_{\mathbf{x}}^T$, $\phi_{\mathbf{x}}(n_{\mathbf{x}} t_{\mathbf{x}}^T + t_{\mathbf{x}} n_{\mathbf{x}}^T)$ plus two modified functions

$$\phi_{\mathbf{x}} \Big|_{\bigcup_{K \in K_{\mathbf{x}}^+} K} t_{\mathbf{x}} t_{\mathbf{x}}^T, \phi_{\mathbf{x}} \Big|_{\bigcup_{K \in K_{\mathbf{x}}^-} K} t_{\mathbf{x}} t_{\mathbf{x}}^T$$

with

$$(4.1) \quad K_{\mathbf{x}}^+ := \cup\{K, \mathbf{x} \in K, K \in \mathcal{T}_h, (\text{mid}(K) - \mathbf{x}) \cdot n_{\mathbf{x}} > 0\}$$

and

$$(4.2) \quad K_{\mathbf{x}}^- := \cup\{K, \mathbf{x} \in K, K \in \mathcal{T}_h, (\text{mid}(K) - \mathbf{x}) \cdot n_{\mathbf{x}} < 0\}.$$

Here $\text{mid}(K)$ denotes the barycentre of K .

Throughout this section, denote the extended discrete stress space on mesh \mathcal{T}_h by $\Sigma(\mathcal{T}_h)$. As explained in Remark 3.1, the same displacement space in (2.5) is still used and here denoted by $V(\mathcal{T}_h)$. Note that the discrete stress space on the initial mesh \mathcal{T}_0 is the original space Σ_h defined in (2.2) on \mathcal{T}_0 ; $\Sigma(\mathcal{T}_h)$ on \mathcal{T}_h is Σ_h in (2.2) on \mathcal{T}_h enriched by those modified basis functions associated with new vertices. It can be easily checked that for any coarse mesh \mathcal{T}_H and its refinement \mathcal{T}_h , it holds $\Sigma(\mathcal{T}_H) \subset \Sigma(\mathcal{T}_h)$.

To establish the adaptive algorithms of the new mixed element, we utilize the a posteriori error estimator in [12]. Let \mathcal{E}_h denote the set of edges of \mathcal{T}_h . For $\phi \in H^1(\Omega; \mathbb{R})$, $v = (v_1, v_2)^T \in H^1(\Omega; \mathbb{R}^2)$, set

$$\text{Curl}\phi := (-\partial\phi/\partial x_2, \partial\phi/\partial x_1), \quad \text{Curl}v := \begin{pmatrix} -\partial v_1/\partial x_2 & \partial v_1/\partial x_1 \\ -\partial v_2/\partial x_2 & \partial v_2/\partial x_1 \end{pmatrix}.$$

The symmetric part of the gradient of a vector field v , denoted by $\epsilon(v)$, is given by $\epsilon(v) := (\nabla v + \nabla^T v)/2$. For $v = (v_1, v_2)^T \in H^1(\Omega; \mathbb{R}^2)$ and $\tau = (\tau_{ij})_{2 \times 2}$, set

$$\text{curl}v := \partial v_2/\partial x_1 - \partial v_1/\partial x_2, \quad \text{curl}\tau = \begin{pmatrix} \partial\tau_{12}/\partial x_1 - \partial\tau_{11}/\partial x_2 \\ \partial\tau_{22}/\partial x_1 - \partial\tau_{21}/\partial x_2 \end{pmatrix}.$$

Denote by $\mathcal{E}_h(\Omega)$ the collection of all interior element edges in \mathcal{T}_h and $\mathcal{E}_h(\Gamma)$ the collection of all element edges on the boundary Γ . For any triangle $K \in \mathcal{T}_h$, let $\mathcal{E}(K)$ denote the set of its edges. Let h_K denote the diameter of the element K and h_e denote the length of the edge e . The jump $[w]_e$ of w across edge $e = K_+ \cap K_-$ reads

$$[w]_e := (w|_{K_+})|_e - (w|_{K_-})|_e.$$

Particularly, if $e \in \mathcal{E}_h(\Gamma)$, $[w]_e := w|_e$. Then the a posteriori error estimator in [12] reads

$$\eta^2(\sigma_h, \mathcal{T}_h) := \sum_{K \in \mathcal{T}_h} \eta_K^2(\sigma_h) + \sum_{e \in \mathcal{E}_h} \eta_e^2(\sigma_h)$$

with

$$\begin{aligned} \eta_K^2(\sigma_h) &:= h_K^4 \|\operatorname{curl} \operatorname{curl}(A\sigma_h)\|_{0,K}^2, \quad \eta_e^2(\sigma_h) := h_e \|\mathcal{J}_{e,1}\|_{0,e}^2 + h_e^3 \|\mathcal{J}_{e,2}\|_{0,e}^2, \\ \mathcal{J}_{e,1} &:= \begin{cases} [(A\sigma_h)t_e \cdot t_e]_e & \text{if } e \in \mathcal{E}_h(\Omega), \\ ((A\sigma_h)t_e \cdot t_e - \partial_{t_e}(u_D \cdot t_e))|_e & \text{if } e \in \mathcal{E}_h(\Gamma_D), \end{cases} \\ \mathcal{J}_{e,2} &:= \begin{cases} [\operatorname{curl}(A\sigma_h) \cdot t_e]_e & \text{if } e \in \mathcal{E}_h(\Omega), \\ (\operatorname{curl}(A\sigma_h) \cdot t_e + \partial_{t_e}(u_D \cdot \nu) - \partial_{t_e}((A\sigma_h)t_e \cdot n_e))|_e & \text{if } e \in \mathcal{E}_h(\Gamma_D). \end{cases} \end{aligned}$$

Suppose (σ, u) denotes the exact solution and $(\sigma_h, u_h) \in \Sigma(\mathcal{T}_h) \times V(\mathcal{T}_h)$ denotes the discrete solution to the nested mixed element method over \mathcal{T}_h . Then, there exist positive constants C_{Rel} and C_{Eff} depending on the shape regularity of \mathcal{T}_h such that

$$(4.3) \quad \|\sigma - \sigma_h\|_A^2 \lesssim C_{Rel}^2 (\eta^2(\sigma_h, \mathcal{T}_h) + \operatorname{osc}^2(f, \mathcal{T}_h)) \quad (\text{reliability}),$$

$$(4.4) \quad \eta^2(\sigma_h, \mathcal{T}_h) \lesssim C_{Eff}^2 \|\sigma - \sigma_h\|_A^2 \quad (\text{efficiency}),$$

The data oscillation reads

$$\operatorname{osc}^2(f, \mathcal{T}_h) := \sum_{K \in \mathcal{T}_h} h_K^2 \|f - Q_h f\|_{0,K}^2,$$

where Q_h is the L^2 orthogonal projection operator onto the discrete displacement space $V(\mathcal{T}_h)$.

Remark 4.1. Note that the stress space from [14, 17] is a subspace of the extended stress space. Therefore, the argument in Theorem 3.1 of [12] can be applied to prove the reliability (4.3), and the argument in Theorem 3.2 of [12] can be applied to prove the efficiency (4.4). The details are omitted in this paper.

4.2. Optimality. Having constructed the new conforming stress spaces on adaptive meshes, this subsection proves the optimal convergence rates of the corresponding adaptive algorithm. For simplicity, the analysis only focuses on the case $\Gamma_N = \emptyset$ and $u_D \equiv 0$.

Algorithm 1: Adaptive algorithm for the nested mixed finite element method.

Given a parameter $0 < \theta < 1$ and an initial mesh \mathcal{T}_0 . Set $m := 0$.

- **SOLVE:** Solve the mixed finite element method on \mathcal{T}_m for the discrete solution $(\sigma_m, u_m) \in \Sigma(\mathcal{T}_m) \times V(\mathcal{T}_m)$.
- **ESTIMATE:** Compute the error indicator $\eta^2(\sigma_m, \mathcal{T}_m)$ piecewise.
- **MARK:** Mark a set $\mathcal{M}_m \subset \mathcal{T}_m$ with minimal cardinality by Dörfler marking such that

$$\eta^2(\sigma_m, \mathcal{M}_m) + \operatorname{osc}^2(f, \mathcal{M}_m) \geq \theta (\eta^2(\sigma_m, \mathcal{T}_m) + \operatorname{osc}^2(f, \mathcal{T}_h)).$$

- **REFINE:** Refine each triangle K with at least one edge in \mathcal{M}_m by the newest vertex bisection to get \mathcal{T}_{m+1} .
 - Set $m := m + 1$ and go to Step **SOLVE**.
-

In [16], the authors present a unified analysis of adaptive mixed finite element methods for a class of problems when the finite element spaces and corresponding a posteriori error

estimates under consideration satisfy five hypotheses. They analyze some vector and non-symmetric mixed elements. This paper generalizes to the symmetric mixed elements. The subsequent contents explain that the nested symmetric mixed element satisfies the five hypotheses in [16], and the fourth hypothesis is an analogy to that in [16], but a new version applied to the symmetric stress space. Suppose \mathcal{T}_h is a refinement of \mathcal{T}_H .

Hypothesis 1. It can be easily checked that discrete spaces $\Sigma(\mathcal{T}_H) \subset \Sigma(\mathcal{T}_h)$ and $\text{div}\Sigma(\mathcal{T}_H) \subset V(\mathcal{T}_H) \subset V(\mathcal{T}_h)$.

Hypothesis 2. The pair of spaces $(\Sigma(\mathcal{T}_h), V(\mathcal{T}_h))$ satisfies the discrete inf-sup condition

$$\|v_h\|_{1,h} \lesssim \sup_{0 \neq \tau_h \in \Sigma(\mathcal{T}_h)} \frac{(\text{div}\tau_h, v_h)}{\|\tau_h\|_0} \text{ for any } v_h \in V(\mathcal{T}_h)$$

with

$$\|v\|_{1,h}^2 := \sum_{K \in \mathcal{T}_h} \|\epsilon(v)\|_{0,K}^2 + \sum_{e \in \mathcal{E}_h} h_e^{-1} \| [v] \|_{0,e}^2.$$

This condition has been proved in [11] for the mixed element from [14, 17] whose stress space is a subspace of the extended stress space $\Sigma(\mathcal{T}_h)$. Hence it is apparently that the inf-sup condition holds for the nested mixed element.

Hypothesis 3. Let Q_H denote the L^2 orthogonal projection operator onto $V(\mathcal{T}_H)$. Then, for any $v_h \in V(\mathcal{T}_h)$,

$$Q_H v_h|_K = v_h|_K \text{ for any } K \in \mathcal{T}_H \cap \mathcal{T}_h$$

and

$$\|v_h - Q_H v_h\|_{0,K} \leq C_U h_K \|v_h\|_{1,h,\Omega_K} \text{ for any } K \in \mathcal{T}_H \setminus \mathcal{T}_h.$$

Here

$$\|v\|_{1,h,\Omega_K}^2 := \sum_{K \in \Omega_K} \|\epsilon(v)\|_{0,K}^2 + \sum_{e \in \mathcal{E}_h \cap (\bigcup_{K \in \Omega_K} \mathcal{E}(K))} h_e^{-1} \| [v] \|_{0,e}^2$$

and

$$\Omega_K := \bigcup_{K' \cap K \neq \emptyset} K'.$$

The proof of Hypothesis 3 for the vector space is similar to that for the scalar space in [20, Lemma 2.8].

Hypothesis 4. Suppose $H_h^2(\Omega)$ (resp. $H_H^2(\Omega)$) denotes some finite element of $H^2(\Omega)$ on mesh \mathcal{T}_h (resp. \mathcal{T}_H). Given $\xi_h \in \Sigma(\mathcal{T}_h)$ with $\text{div}\xi_h = 0$, there exist $\phi_h \in H_h^2(\Omega)$ and operator $\Pi_{H,\nabla^2} : H_h^2(\Omega) \rightarrow H_H^2(\Omega)$ such that

$$(4.5) \quad \xi_h = \text{CurlCurl}\phi_h \text{ and } \text{CurlCurl}\Pi_{H,\nabla^2}\phi_h \in \Sigma(\mathcal{T}_H).$$

Moreover, $\psi := \phi_h - \Pi_{H,\nabla^2}\phi_h \in H^2(\Omega)$ satisfies the estimates

$$(4.6) \quad \begin{cases} \psi|_K = 0 \text{ for any } K \in \mathcal{T}_H \cap \mathcal{T}_h, \\ (\sum_{K \in \mathcal{T}_H} \|h_K^{-2}\psi\|_{0,K}^2)^{1/2} \lesssim \|\text{CurlCurl}\phi_h\|_0, \\ (\sum_{e \in \mathcal{E}_H} \|h_e^{-3/2}\psi\|_{0,e}^2)^{1/2} \lesssim \|\text{CurlCurl}\phi_h\|_0, \\ (\sum_{e \in \mathcal{E}_H} \|h_e^{-1/2}\text{Curl}\psi \cdot n_e\|_{0,e}^2)^{1/2} \lesssim \|\text{CurlCurl}\phi_h\|_0. \end{cases}$$

Recall the subdomains K_x^+ defined in (4.1) and K_x^- in (4.2). The following conforming finite element spaces from [10] approximating $H^2(\Omega)$ are analogous to the higher order

Argyris finite element spaces by a modification around the vertices. Define

$$S^k(\mathcal{T}_h) := \{v \in L^2(\Omega) : v|_K \in P_k(K), \forall K \in \mathcal{T}_h, v \text{ and its all first derivatives are continuous on the vertices, } \nabla v \text{ are continuous on the edges, } \nabla^2 v \text{ are continuous at the vertices of } \mathcal{T}_0, n_x^T \nabla^2 v t_x \text{ and } t_x^T \nabla^2 v t_x \text{ are continuous at the vertices } x \in \mathcal{X}_V(\mathcal{T}_h) \setminus \mathcal{X}_V(\mathcal{T}_0), n_x^T \nabla^2 v n_x \text{ is continuous at } x \text{ in } K_x^+ \text{ and at } x \text{ in } K_x^- \text{ for the vertices } x \in \mathcal{X}_V(\mathcal{T}_h) \setminus \mathcal{X}_V(\mathcal{T}_0)\}.$$

Unlike functions in the Argyris finite element space, the component $n_x^T \nabla^2 v n_x$ of the second derivatives of function $v \in S^k(\mathcal{T}_h)$ is not necessarily continuous at the vertex $x \in \mathcal{X}_V(\mathcal{T}_h) \setminus \mathcal{X}_V(\mathcal{T}_0)$. The exact sequence reads

$$(4.7) \quad P_1(\Omega; \mathbb{R}) \rightarrow S^{k+2}(\mathcal{T}_h) \xrightarrow{\text{CurlCurl}} \Sigma(\mathcal{T}_h) \xrightarrow{\text{div}} V(\mathcal{T}_h).$$

This holds because $\text{CurlCurl}S^{k+2}(\mathcal{T}_h) \subset \Sigma(\mathcal{T}_h)$. In addition, note that the high order Argyris element, the mixed element from [14, 17] and $V(\mathcal{T}_h)$ form an exact sequence. Both of the new spaces $S^{k+2}(\mathcal{T}_h)$ and $\Sigma(\mathcal{T}_h)$ are enhanced by adding the same number of degrees of freedom, which shows the exactness of the sequence (4.7). Let $H_h^2(\Omega) := S^{k+2}(\mathcal{T}_h)$ and Π_{H,∇^2} be the quasi-interpolation operator in [10], then (4.5) holds. Let $\psi = \phi_h - \Pi_{H,\nabla^2}\phi_h$ and the estimates in (4.6) can be achieved by Theorem 2 of [10] and trace inequalities.

Hypothesis 5. There exists a reliable and efficient a posteriori error estimator, which has shown in (4.3) and (4.4).

Since the Hypothesis 4 is different from that in [16], it requires to prove a similar result as in [16, Lemma 3.1] which implies the discrete reliability. To this end, define the kernel space on \mathcal{T}_h

$$Z_h(0) := \{\tau \in \Sigma(\mathcal{T}_h) \mid \text{div}\tau = 0\}.$$

Lemma 4.2. *Given $f \in L^2(\Omega; \mathbb{R}^2)$, let (σ_H, u_H) be the solution to the discrete problem over the triangulation \mathcal{T}_H , and let ξ_h be the A projection of σ_H onto the space $Z_h(0)$ with*

$$(A\xi_h, \tau_h) = (A\sigma_H, \tau_h) \text{ for any } \tau_h \in Z_h(0).$$

Then it holds that

$$\|\xi_h\|_A^2 \lesssim \eta^2(\sigma_H, \mathcal{T}_H \setminus \mathcal{T}_h).$$

Proof. By the definition of ξ_h ,

$$(4.8) \quad \|\xi_h\|_A^2 = (A\xi_h, \xi_h) = (A\sigma_H, \xi_h) = (A\sigma_H, \xi_h - \tau_H)$$

holds for any $\tau_H \in Z_H(0)$. Since $\text{div}\xi_h = 0$, it follows from Hypothesis 4 that there exists $\phi_h \in H_h^2(\Omega)$ such that $\xi_h = \text{CurlCurl}\phi_h$. Hence selecting $\tau_H = \text{CurlCurl}\Pi_{H,\nabla^2}\phi_h \in \Sigma_H$ implies that there exists $\psi \in H^2(\Omega; \mathbb{R}^2)$ such that

$$(4.9) \quad \xi_h - \tau_H = \text{CurlCurl}(\phi_h - \Pi_{H,\nabla^2}\phi_h) = \text{CurlCurl}\psi$$

with ψ satisfying (4.6). A summary of (4.8), (4.9) and (4.6) shows

$$\|\xi_h\|_A^2 = (A\sigma_H, \text{CurlCurl}\psi) = (A\sigma_H, \text{CurlCurl}\psi)_{\mathcal{T}_H \setminus \mathcal{T}_h}.$$

The integration by parts plus (4.6) lead to

$$\begin{aligned} \|\xi_h\|_A^2 &= \sum_{K \in \mathcal{T}_H \setminus \mathcal{T}_h} \left((\text{curlcurl}(A\sigma_H), \psi)_K + \sum_{e \in \mathcal{E}(K)} (\langle A\sigma_H t_e \cdot t_e, \text{Curl}\psi \cdot t_e \rangle_e - \langle \text{curl}(A\sigma_H) \cdot t_e, \psi \rangle_e) \right. \\ &\quad \left. + \sum_{e \in \mathcal{E}(K)} \langle A\sigma_H t_e \cdot n_e, \text{Curl}\psi \cdot n_e \rangle_e \right). \end{aligned}$$

Since $A\sigma_H t_e \cdot n_e = A\sigma_H n_e \cdot t_e$ is continuous across interior edge e . This implies

$$\begin{aligned} \sum_{K \in \mathcal{T}_H \setminus \mathcal{T}_h} \sum_{e \in \mathcal{E}(K)} \langle A\sigma_H t_e \cdot n_e, \text{Curl}\psi \cdot n_e \rangle_e &= - \sum_{K \in \mathcal{T}_H \setminus \mathcal{T}_h} \sum_{e \in \mathcal{E}_H(\Gamma) \cap \mathcal{E}(K)} \langle A\sigma_H t_e \cdot n_e, \partial_{t_e} \psi \rangle_e \\ &= \sum_{K \in \mathcal{T}_H \setminus \mathcal{T}_h} \sum_{e \in \mathcal{E}_H(\Gamma) \cap \mathcal{E}(K)} \langle \partial_{t_e} (A\sigma_H t_e \cdot n_e), \psi \rangle_e, \end{aligned}$$

where the fact ψ vanishing at the boundary vertices is used. Therefore,

$$\begin{aligned} \|\xi_h\|_A^2 &\lesssim \left(\sum_{K \in \mathcal{T}_H \setminus \mathcal{T}_h} \left(\|h_K^2 \text{curlcurl}(A\sigma_H)\|_{0,K}^2 + \sum_{e \in \mathcal{E}(K)} \|h_e^{1/2} [A\sigma_H t_e \cdot t_e]\|_{0,e}^2 \right. \right. \\ &\quad + \sum_{e \in \mathcal{E}(K) \cap \mathcal{E}_H(\Omega)} \|h_e^{3/2} [\text{curl}(A\sigma_H) \cdot t_e]\|_{0,e}^2 \\ &\quad \left. \left. + \sum_{e \in \mathcal{E}_H(\Gamma) \cap \mathcal{E}(K)} \|h_e^{3/2} (\text{curl}(A\sigma_H) \cdot t_e - \partial_{t_e} (A\sigma_H t_e \cdot n_e))\|_{0,e}^2 \right) \right)^{1/2} \|\xi\|_0. \end{aligned}$$

Since $\text{div}\xi_h = 0$, it was proved in [7, Proposition 9.1.1] that

$$\|\xi_h\|_0 \lesssim \|\xi_h\|_A,$$

which immediately implies

$$\begin{aligned} \|\xi_h\|_A^2 &\lesssim \sum_{K \in \mathcal{T}_H \setminus \mathcal{T}_h} \left(\|h_K^2 \text{curlcurl}(A\sigma_H)\|_{0,K}^2 + \sum_{e \in \mathcal{E}(K)} \|h_e^{1/2} [A\sigma_H t_e \cdot t_e]\|_{0,e}^2 \right. \\ &\quad + \sum_{e \in \mathcal{E}(K) \cap \mathcal{E}_H(\Omega)} \|h_e^{3/2} [\text{curl}(A\sigma_H) \cdot t_e]\|_{0,e}^2 \\ &\quad \left. + \sum_{e \in \mathcal{E}_H(\Gamma) \cap \mathcal{E}(K)} \|h_e^{3/2} (\text{curl}(A\sigma_H) \cdot t_e - \partial_{t_e} (A\sigma_H t_e \cdot n_e))\|_{0,e}^2 \right). \end{aligned}$$

This concludes the proof. \square

Define the approximation class \mathbb{A}_s as

$$\mathbb{A}_s = \left\{ (\sigma, f) : |\sigma, f|_s < \infty \text{ with } |\sigma, f|_s := \sup_{N>0} \inf_{\#\mathcal{T}=\#T_0 \leq N} \inf_{\tau \in \Sigma(\mathcal{T})} \|\sigma - \tau\|_A^2 + \text{osc}^2(f, \mathcal{T}) \right\}.$$

The convergence results of the adaptive algorithm are presented as follows.

Theorem 4.3. *Given $f \in L^2(\Omega; \mathbb{R}^2)$, let (σ, u) be the exact solution of the linear elasticity problem, and (σ_k, u_k) and (σ_{k-1}, u_{k-1}) be the discrete solutions over the nested triangulations \mathcal{T}_k and \mathcal{T}_{k-1} , respectively. Then there exist positive constants $0 < \alpha < 1$, $\beta > 0$, $\gamma > 0$ such that*

$$e_k \leq \alpha e_{k-1}$$

with

$$e_k = \|\sigma - \sigma_k\|_A^2 + \gamma \eta^2(\sigma_k, \mathcal{T}_k) + (\beta + \gamma) \text{osc}^2(f, \mathcal{T}_k).$$

Theorem 4.4. *Let \mathcal{M}_k be a set of marked elements with minimal cardinality, (σ, u) the solution of (2.1), and $(\mathcal{T}_k, \Sigma(\mathcal{T}_k) \times V(\mathcal{T}_k), \sigma_k, u_k)$ the sequence of triangulations, finite element spaces, and discrete solutions produced by the adaptive finite element methods with the marking parameter θ . Then it holds that*

$$\|\sigma - \sigma_N\|_A^2 + \text{osc}^2(f, \mathcal{T}_N) \lesssim |\sigma, f|_s (\#\mathcal{T}_N - \#\mathcal{T}_0)^{-s} \text{ for } (\sigma, f) \in \mathbb{A}_s.$$

5. NUMERICS

Through four numerical experiments, this section compares the mixed element of $k = 3$ from [14, 17] (also introduced in Section 2) with the novel mixed element in this paper with an extended stress space. The first three examples test the remedy of relaxing the C^0 continuity at corner vertices as in Subsect. 3.2 on uniform and adaptive meshes. The fourth example demonstrates convergence rates of the adaptive mixed finite element method in Section 4.

5.1. A benchmark problem over an L-shaped domain with treatment of corners on uniform meshes. Consider the model problem on the rotated L-shaped domain $\Omega \subset \mathbb{R}^2$ as depicted in Figure 5.1. The exact solution reads in polar coordinates

$$u_r(r, \phi) = \frac{r^\alpha}{2\mu}(-(\alpha + 1) \cos((\alpha + 1)\phi) + (C_2 - \alpha - 1)C_1 \cos((\alpha - 1)\phi)),$$

$$u_\phi(r, \phi) = \frac{r^\alpha}{2\mu}((\alpha + 1) \sin((\alpha + 1)\phi) + (C_2 + \alpha - 1)C_1 \sin((\alpha - 1)\phi)).$$

The constants are $C_1 := -\cos((\alpha + 1)\omega)/\cos((\alpha - 1)\omega)$ and $C_2 := 2(\lambda + 2\mu)/(\lambda + \mu)$, where $\alpha = 0.544483736782$ is the positive solution of $\alpha \sin(2\omega) + \sin(2\omega\alpha) = 0$ for $\omega = 3\pi/4$ and with Lamé parameter λ and μ according to the elasticity modulus is $E = 10^5$ and the Poisson's ratio $\nu = 0.499$. The volume force and the Neumann boundary data vanish, and the Dirichlet boundary conditions are taken from the exact solution. The exact solution exhibits a strong singularity at the origin \mathbf{a} .

The sequence of meshes is generated uniformly by the initial mesh from Figure 5.1. It is unnecessary to deal with the degrees of freedom at corner vertices due to the zero Neumann boundary data. However, considering the singularity of the exact solution at \mathbf{a} , we would like to investigate the performance of the mixed element method in [17] after relaxing the C^0 continuity at \mathbf{a} as in Subsection 3.2. Table 5.1 demonstrates that after the remedy, the errors of $\|\sigma - \sigma_h\|_A$ and $\|u - u_h\|_0$ are largely reduced.

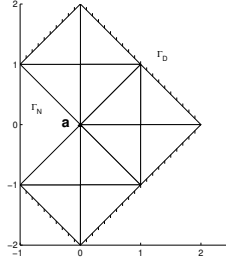


FIGURE 5.1. Initial mesh for the L-shaped domain

5.2. Cook's membrane problem with treatment of corners on uniform meshes. Recall Cook's membrane problem introduced in Subsect. 3.2. In this example, the elasticity modulus is $E = 10^5$ and the Poisson's ratio $\nu = 0.499$. The initial mesh is depicted in Figure 5.2. This example relaxes the C^0 continuity at \mathbf{a} and \mathbf{b} . Since the exact solution is unknown, the fine grid approximation is computed by the standard continuous P_5 -FEM on twice uniform refinements of the grid for the last level. Table 5.2 shows that after the remedy, the errors are reduced, especially on the coarse mesh.

TABLE 5.1. A benchmark problem on L-shaped domain on uniform meshes

Mesh	$\ \sigma - \sigma_h\ _A$			
	Before remedy	Order	After remedy	Order
1	7.3062E-03		2.4379E-03	
2	5.2168E-03	0.4860	1.7144E-03	0.5079
3	3.6276E-03	0.5241	1.1811E-03	0.5375
4	2.5075E-03	0.5328	8.1151E-04	0.5415
5	1.7280E-03	0.5371	5.5692E-04	0.5431
$\ u - u_h\ _0$				
1	6.5608E-06		1.1561E-06	
2	3.4583E-06	0.9238	5.1230E-07	1.1742
3	1.6759E-06	1.0452	2.1802E-07	1.2325
4	8.0297E-07	1.0615	9.5757E-08	1.1871
5	3.8181E-07	1.0725	4.3159E-08	1.1497

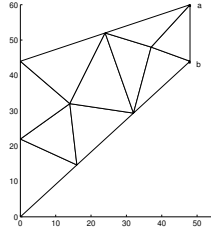


FIGURE 5.2. Initial mesh for Cook's membrane problem

TABLE 5.2. Cook's membrane problem on uniform meshes

Mesh	$\ \sigma - \sigma_h\ _A$			
	Before remedy	Order	After remedy	Order
1	0.0505		0.0245	
2	0.0277	0.8648	0.0159	0.6227
3	0.0156	0.8262	0.0104	0.6213
4	0.0090	0.7925	0.0067	0.6261
$\ u - u_h\ _0$				
1	9.2751E-03		9.8907E-04	
2	4.6433E-03	0.9982	4.1703E-04	1.2459
3	2.3348E-03	0.9919	1.7483E-04	1.2542
4	1.1760E-03	0.9894	7.3007E-05	1.2599

5.3. Cook's membrane problem with treatment of corners on adaptive meshes. This example tests Cook's membrane problem by adaptive mixed finite elements. The elasticity modulus is $E = 10^5$ and Poisson's ration is $\nu = 0.499$. The discrete stress and displacement before remedy is denoted by σ_h^N and η^N , respectively. Due to the general Neumann boundary conditions, the least squares method is employed in this case to decide the values of stress at the two right corners. The discrete solutions after the relaxation of the C^0 continuity at a and b are denoted by σ_h^Y and η^Y . The approximations by the standard

continuous P_5 element on the very fine mesh are computed as the reference solutions. The results are shown in Figure 5.3. Since the error of the inconsistent boundary conditions dominates at the initial steps, the result before remedy is worse than after remedy. After several refinements, the results are almost the same since the error of inconsistency has deduced greatly.

Below describes the special mesh refinement in the adaptive algorithm. Given a mesh \mathcal{T}_h , in order to relax the C^0 continuity at corner vertices, each triangle K around corner vertices is divided into three sub-triangles K_i , $i = 1, 2, 3$ as explained in Remark 3.2. This results in a new mesh $\widehat{\mathcal{T}}_h$. Solve the problem by the new mixed element method in Subsect. 3.2 on $\widehat{\mathcal{T}}_h$. In the mesh refinement step, instead from the mesh $\widehat{\mathcal{T}}_h$, the next mesh is generated by the newest vertex bisection from the mesh \mathcal{T}_h . This will avoid the angles of triangles around corners smaller and smaller in the loops. The a posteriori error estimator is with these terms associated with the sub-triangles added to the original triangles, i.e. $\eta(\sigma_h, K)^2 = \sum_{i=1}^3 \eta(\sigma_h, K_i)^2$.

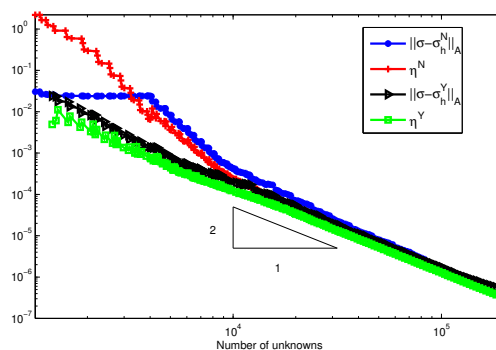


FIGURE 5.3. Errors $\|\sigma - \sigma_h\|_A$ and $\eta(\sigma_h, \mathcal{T}_h)$ vs #dofs for Cook's membrane problem

5.4. Comparison of adaptivity algorithms for two mixed elements. This example compares the non-nested mixed element method from [17] with the nested mixed element method in Section 4 on adaptive meshes for the benchmark problem in Subsect. 5.1. The results are shown in Figure 5.4. Let σ_h^O and η^O denote the discrete stress and the a posteriori error estimator of the former element, and σ_h^M and η^M denote the results of the latter element. Figure 5.4 presents the convergence history plot and illustrates that there is not much difference between these two elements.

REFERENCES

- [1] D. N. Arnold and G. Awanou, Rectangular mixed finite elements for elasticity, *Math. Models Methods Appl. Sci.* 15 (2005), 1417–1429.
- [2] D. Arnold, G. Awanou and R. Winther. Finite elements for symmetric tensors in three dimensions. *Math. Comp.* 77 (2008), 1229–1251.
- [3] D. N. Arnold, F. Brezzi and J. Douglas, Jr., PEERS: A new mixed finite element for plane elasticity, *Jpn. J. Appl. Math.*, 1 (1984), 347–367.
- [4] D.N. Arnold, R. Falk and R. Winther, Mixed finite element methods for linear elasticity with weakly imposed symmetry, *Math. Comp.*, 76 (2007), no. 260, 1699–1723.
- [5] D. N. Arnold and R. Winther. Mixed finite element for elasticity. *Numer. Math.* 92 (2002), 401–419.

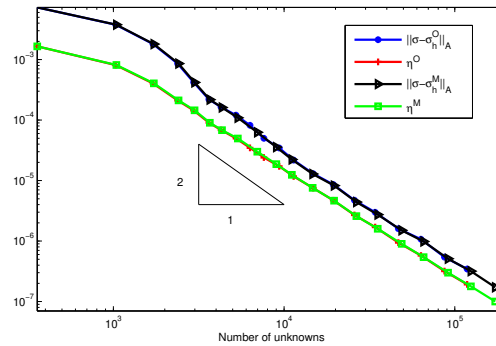


FIGURE 5.4. Errors $\|\sigma - \sigma_h\|_A$ and $\eta(\sigma_h, \mathcal{T}_h)$ vs #dofs for the problem over an L-shaped domain

- [6] D. Boffi, F. Brezzi and M. Fortin, Reduced symmetry elements in linear elasticity, *Commun. Pure Appl. Anal.* 8 (2009), no. 1, 95–21.
- [7] D. Boffi, F. Brezzi, and M. Fortin. *Mixed finite element methods and applications*, Springer, Heidelberg, 2013.
- [8] C. Carstensen, D. Günther, J. Reininghaus, and J. Thiele. The Arnold-Winther mixed FEM in linear elasticity. part I: Implementation and numerical verification, *Comput. Methods Appl. Mech. Engrg.* 197 (2008), 3014–3023.
- [9] C. Carstensen, J. Gedicke. Robust residual-based a posteriori Arnold-Winther mixed finite element analysis in elasticity, *Comput. Methods Appl. Mech. Engrg.* 300 (2016), 245–264.
- [10] C. Carstensen and J. Hu. An extended Argyris finite element method with optimal standard adaptive and multigrid V-cycle algorithms. preprint
- [11] L. Chen, J. Hu, and X. Huang. Fast auxiliary space preconditioner for linear elasticity in mixed form. *Math. Comp.* 87 (2018), 1601–1633.
- [12] L. Chen, J. Hu, X. Huang and H. Man. Residual-based a posteriori error estimates for symmetric conforming mixed finite elements for linear elasticity problems. *Sci. China Math.* 61 (2018), 973–992.
- [13] H. C. Hu, On some variational principles in the theory of elasticity and theory of plasticity, *Acta Phys. Sin.*, 10 (1954), pp. 259–290.
- [14] J. Hu. Finite element approximations of symmetric tensors on simplicial grids in \mathbb{R}^n : the higher order case. *J. Comput. Math.* 33 (2015), 283–296.
- [15] J. Hu, A new family of efficient conforming mixed finite elements on both rectangular and cuboid meshes for linear elasticity in the symmetric formulation, *SIAM J. Numer. Anal.*, 53(2015), pp. 1438C1463.
- [16] J. Hu and G. Yu. A unified analysis of quasi-optimal convergence for adaptive mixed finite element methods. *SIAM J. Numer. Anal.* 56 (2018), 296–316.
- [17] J. Hu and S. Zhang. A family of conforming mixed finite elements for linear elasticity on triangular grids. arXiv:1406.7457, 2014.
- [18] J. Hu and S. Zhang. A family of symmetric mixed finite elements for linear elasticity on tetrahedral grids. *Sci. China Math.* 58 (2015), 297–307.
- [19] J. Hu and S. Zhang. Finite element approximations of symmetric tensors on simplicial grids in \mathbb{R}^n : The lower order case. *Math. Models Methods Appl. Sci.* 26 (2016), 1649–1669.
- [20] J. Huang and Y. Xu. Convergence and complexity of arbitrary order adaptive mixed element methods for the Poisson equation. *Sci. China Math.* 55 (2012), 1083–1098.
- [21] C. Johnson and B. Mercier. Some equilibrium finite element methods for two-dimensional elasticity problems, *Numer. Math.* 30 (1978), 103–116.

LMAM AND SCHOOL OF MATHEMATICAL SCIENCES, PEKING UNIVERSITY, BEIJING 100871, P. R. CHINA. HJJUN@MATH.PKU.EDU.CN

LMAM AND SCHOOL OF MATHEMATICAL SCIENCES, PEKING UNIVERSITY, BEIJING 100871, P. R. CHINA. MARUIPKU@GMAIL.COM